Theoretical Investigation of Influence of Mechanical Stress on Magnetic Properties of Ferromagnetic/Antiferromagnetic Bilayers Deposited on Flexible Substrates *

Yu-Hao Bai(白宇浩)[1,2], Xia Wang(王霞)[2], Lin-Ping Mu(穆林平)[1], Xiao-Hong Xu(许小红)[2**]

[1]*College of Physics and Electronic Information, Shanxi Normal University, Linfen 041004*

[2]*School of Chemistry and Materials Science, Key Laboratory of Magnetic Molecules and Magnetic Information Materials (Ministry of Education), Shanxi Normal University, Linfen 041004*

(Received 25 March 2016)

Effect of mechanical stress on magnetic properties of an exchange-biased ferromagnetic/antiferromagnetic bilayer deposited on a flexible substrate is investigated. The hysteresis loops with different magnitudes and orientations of the stress can be classified into three types. The corresponding physical conditions for each type of the loop are deduced based on the principle of minimal energy. The equation of the critical stress is derived, which can judge whether the loops show hysteresis or not. Numerical calculations suggest that except for the magnitude of the mechanical stress, the relative orientation of the stress is also an important factor to tune the exchange bias effect.

PACS: 75.30.Gw, 75.60.Jk, 75.70.−i DOI: 10.1088/0256-307X/33/8/087501

Exchange bias (EB)[1] is one of the important topics in modern magnetism due to its important technological applications.[2−10] Many studies have revealed that the relative magnitude and orientation of the magnetic anisotropies influence the EB effect significantly.[11−16] The configuration of the anisotropy will be changed by introducing a new anisotropy with the help of several technical methods, such as oblique deposition,[17−20] field annealing treatment,[21] lattice mismatch strain,[22,23] the deposition of ferromagnetic (FM)/antiferromagnetic (AFM) system on the flexible or ferroelectric substrate,[24−27] as well as the electric-field-controlled magnetic anisotropies by depositing an FM layer on a ferroelectric substrate.[28−32]

A tunable strain-induced uniaxial anisotropy caused by bending substrates has been observed in many magnetic films or heterostructures.[24−27,33−35] For example, by exploiting the specially designed sample holder, Han *et al.* have found that the coercivity $H_{\rm C}$ was significantly affected by the stress when depositing NiFe/NiO bilayer onto the rigid Si wafers, while the exchange bias field $H_{\rm EB}$ was not apparently changed.[34,35] With the remarkable clamping effect, the induced strain was too small to tune the magnetic properties effectively. Recently, Zhang *et al.* have studied the effect of the stress on the EB of FeGa/IrMn heterostructures deposited on a flexible polyethylene terephthalate (PET) substrate.[33] Good deformability of the flexible substrate eliminates the clamping effect effectively, and a larger strain (stress) was successfully introduced.[33]

Nevertheless, in the work of Zhang *et al.*, the pinning direction (PD), i.e., the orientation of the magnetic field during the deposition of FM/AFM bilayers, is always parallel or perpendicular to the applied strain. This special geometry of the anisotropy restricts the comprehensive understanding of the effect of the stress on the EB effect. Actually, for a rectangular flexible substrate, the bilayer can be deposited on the flexible substrate under a magnetic field, which is applied along an angle β with the length direction of the sample, then the applied stress will be introduced by inward and outward bending of the heterostructures along its length direction. It will bring about various configurations of the anisotropies by varying the orientations of the depositing field and the EB can be effectively tuned. In this Letter, we perform a theoretical investigation of effects of stress on magnetic properties of an exchange-biased ferromagnetic/antiferromagnetic bilayer deposited on a flexible substrate. Compared with the previous theoretical works,[36,37] we focus on the different types of the hysteresis loops.

The FM/AFM bilayer with an uncompensated interface is assumed to lie at x–y plane. The magnetic field during the deposition is applied along the angle of β with respect to positive x semiaxis. It gives rise to a collinear unidirectional anisotropy $K_{\rm E}$ and uniaxial anisotropy $K_{\rm U}$. The stress σ is induced by outward (tensile stress, $\sigma > 0$) or inward (compressive stress, $\sigma < 0$) bending of the flexible substrate along the x-axis. The external field H is applied along the y-axis, i.e., perpendicular to the strain to ensure that it is always applied in the plane of the heterostructures. The geometries of the various anisotropies as well as the schematic diagram of the stress are illustrated in Figs. 1(a)–1(c).

*Supported by the Youth Science Foundation of Shanxi Province under Grant No 2013021010-3, the National Natural Science Foundation of China under Grant Nos 61434002 and 11404202.

**Corresponding author. Email: xuxh@dns.sxnu.edu.cn

© 2016 Chinese Physical Society and IOP Publishing Ltd

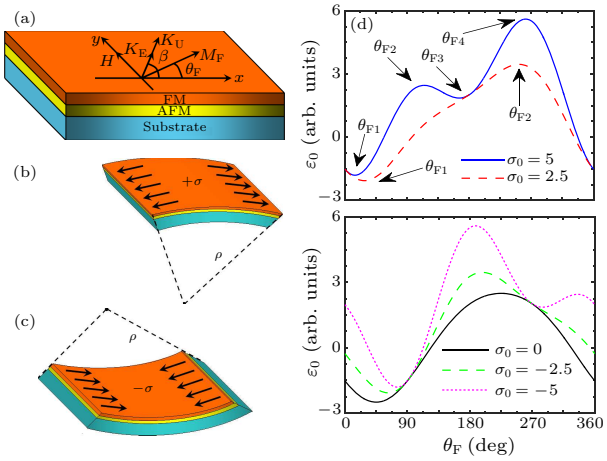

Fig. 1. (Color online) The geometries of the magnetic anisotropies, the mechanical stress, the external field as well as their orientations used in the numerical calculations. (a) No stress is applied. (b) The tensile-stressed state of the bilayer by outward bending the heterostructure. (c) The compressive-stressed state of the bilayer by inward bending the heterostructure. (d) The dependence of the initial magnetic energy of the FM/AFM bilayer ε_0 on the ferromagnetic magnetization orientations θ_F at various values of the stress. The positions of the intrinsic easy axes θ_{F1}, θ_{F3} and the intrinsic hard axes θ_{F2}, θ_{F4} for the bistable and monostable states are indicated by the arrows. The parameters $J = 2.5$, $\beta = 45°$ are taken in the numerical results.

The coherent rotation model has been confirmed to provide an appropriate description of the exchange-bias behaviors,[11–16,23] although it relies only on the rotation of the magnetization and does not consider the magnetic domain nucleation and propagation.[38] Moreover, it has been employed to investigate the mechanical stress effect on the exchange-biased heterostructures grown in flexible[33] and rigid[34,35] substrates. The free energy per unit area of the bilayers in this model can be written as[33]

$$E = K_U t_F \sin^2(\beta - \theta_F) - K_E \cos(\beta - \theta_F) + K_\sigma \cos^2\theta_F - H M_F t_F \sin\theta_F. \quad (1)$$

The first and second terms are the uniaxial and unidirectional anisotropy energies of the FM layer, and t_F is the thickness. The third term refers to the strain-induced anisotropy energy, and K_σ is the corresponding anisotropy constant, which is given by $-\frac{3}{2}\sigma\lambda_s t_F$, where λ_s is the saturated magnetostriction coefficient. The stress can be expressed by $\sigma = sE_f/(1-\nu^2)$, with E_f being Young's module, and ν the Poisson ratio. Here s is the strain, which is determined by $s = d/2\rho$, where d denotes the total thickness of both substrate and the FM/AFM bilayer, and ρ is the curvature radii of the heterostructure.[24–26] We suppose that the FM layer has a positive magnetostriction coefficient. Hence, the easy direction of strain-induced anisotropy is determined by the direction of the tensile stress.[24–26] Finally, the last term stands for the Zeeman energy. Normalizing each energy term by $2K_U t_F$, we obtain

$$\varepsilon = \frac{1}{2}\sin^2(\beta - \theta_F) - J\cos(\beta - \theta_F) - \frac{1}{2}\sigma_0\cos^2\theta_F - h\sin\theta_F, \quad (2)$$

where $J = K_E/2K_U t_F$ stands for the reduced exchange coupling constant, $\sigma_0 = K_\sigma/K_U = 3\lambda_s\sigma/2K_U$ is the reduced stress, $h = H/H_A$ and $H_A = 2K_U/M_F$ are defined respectively as the normalized field and the uniaxial anisotropy field. Combining the uniaxial anisotropy and strain-induced anisotropy into an equivalent uniaxial anisotropy,[37] ε can be rewritten as

$$\varepsilon = \frac{1}{4}(1 - \sigma_0 - A) + \frac{1}{2}A\sin^2(\theta_F - \gamma) - J\cos(\beta - \theta_F) - h\sin\theta_F, \quad (2a)$$

where A and γ indicate the magnitude and the orientation of the effective uniaxial anisotropy, respectively, which are expressed as

$$A = \sqrt{1 + 2\sigma_0\cos 2\beta + \sigma_0^2}, \qquad \tan 2\gamma = \frac{\sin 2\beta}{\cos(2\beta) + \sigma_0}. \quad (2b)$$

Firstly, we investigate the initial state of the system when H is absent. The energy density $\varepsilon_0 = \varepsilon(h = 0)/A$ can be written as

$$\varepsilon_0 = \frac{1}{4A}(1 - \sigma_0 - A) + \frac{1}{2}\sin^2(\theta_F - \gamma) - j\cos(\beta - \theta_F), \quad (2c)$$

where $j = J/A$ is defined as the normalized exchange-coupling constant. This initial energy with the above forms has been discussed in our previous works.[39,40] It does not yield the new physics but a constant term $(1 - A - \sigma_0)/4A$. Consequently, some conclusions can also be valid in this work. For example, bistable and monostable states will also be existent.[39,40]

The dependence of the initial magnetic energy on the orientation of M_F is shown in Fig. 1(d), using the parameters of Zhang*et al.* $H_E = K_E/M_F = 100$ Oe, $H_A = 2K_U/M_F = 40$ Oe, $H_\sigma = K_\sigma/M_F = -100$–$+100$ Oe, i.e., $J = K_E/2K_U = 2.5$ and $\sigma_0 = -5$–$+5$.[33] The determined equation of the critical parameter j_C above which the bilayer makes the transition from bistable to monostable state is given by

$$j_C = \left[\frac{1}{\cos^{2/3}(\beta - \gamma) + \sin^{2/3}(\beta - \gamma)}\right]^{3/2}. \quad (2d)$$

Additionally, the critical stress σ_{0C} can also be derived from Eq. (2d) by expressing the parameters j and γ with functions of J, σ_0 and β,

$$3 \times \left(\frac{\sigma_{0C}\sin 2\beta}{2A}\right)^{2/3}\left[\left(\frac{1 + \sigma_{0C}\cos 2\beta + A}{2\cdot A}\right)^{1/3} + \left(\frac{-1 - \sigma_{0C}\cos 2\beta + A}{2A}\right)^{1/3}\right] = \frac{A^2 - J^2}{J^2}. \quad (2e)$$

As shown in Fig. 2, four different configurations will be shown. The schematic diagrams about the positions of the intrinsic easy and hard axes in different configurations are also given. These axes are defined as the orientation of $M_{\rm F}$ for the energy minimum and maximum, respectively.[39,40] With the assistant of these schematic diagrams, the hysteresis loops with different stresses will be obtained by solving Eq. (2) based on the principle of minimal energy. Here $H_{\rm EB}$ and $H_{\rm C}$ will be extracted from the formulas of $H_{\rm EB} = (H_{\rm CL} + H_{\rm CR})/2$ and $H_{\rm C} = (H_{\rm CR} - H_{\rm CL})/2$, where $H_{\rm CL}$ and $H_{\rm CR}$ represent respectively the coercive fields of the descending and ascending branches of the hysteresis loops.[40]

Figure 3 shows the numerical results of the calculated hysteresis loops. They can be classified into three different types. Type I: the shift presents while no coercivity occurs, i.e., $H_{\rm CL} = H_{\rm CR}$. Type Ⅱ: the loops display a coercivity while both $H_{\rm CL}$ and $H_{\rm CR}$ present the same signs, i.e., either positive or negative sign is shown. Type Ⅲ: the loops exhibit a coercivity, while the sign of $H_{\rm CL}$ is different from that of $H_{\rm CR}$, i.e., $H_{\rm CL} < 0$ and $H_{\rm CR} > 0$. It should be stressed that type I hysteresis loop has been observed in some exchange-biased systems.[11,40–42] Additionally, these types of loops have also been found in the calculated results (see Fig. 4 in Ref. [33]). On the other hand, the loops for $(\sigma_0, +\beta)$ are symmetrical with that for $(\sigma_0, -\beta)$. They have the same width but the reverse shift. Hence, we only need to consider the case of $\beta < 0$ as displayed in Fig. 2.

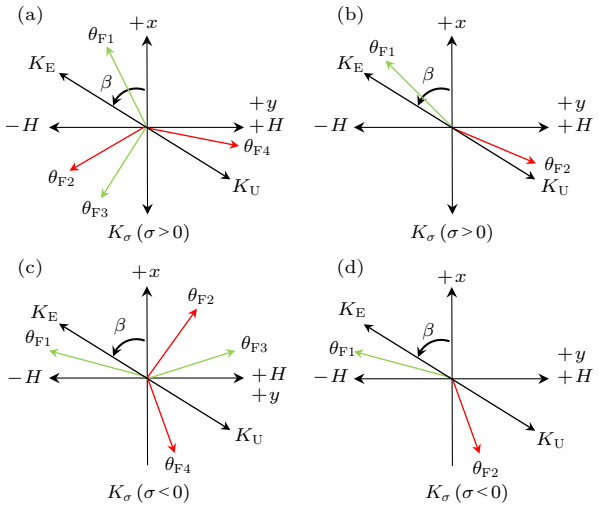

Fig. 2. The different configurations of the intrinsic easy and hard axes when the exchange-biased FM/AFM bilayer is in the bistable state for the tensile stress (a), the monostable state for the tensile stress (b), the bistable state for the compressive stress (c), and the monostable state for the compressive stress (d).

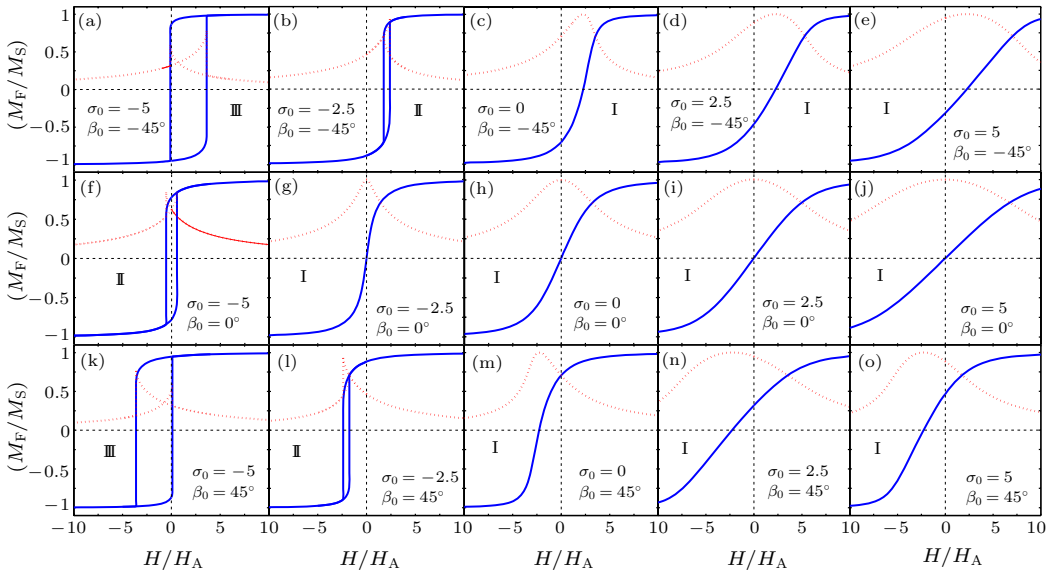

Fig. 3. The calculated hysteresis loops with various magnitudes and orientations of the stress. The parallel ($M_{\rm L}$) and perpendicular components ($M_{\rm T}$) of $M_{\rm F}$ to the applied field H are indicated by the solid and dashed lines, respectively. The symbols I, Ⅱ and Ⅲ represent the different types of the hysteresis loops. The parameters are taken as $J = 2.5$, and the values σ_0 and β are indicated in each hysteresis loop.

After analyzing the magnetization reversal processes, we can explain how these types of loops occur. For example, when the bilayer is in the bistable state for the compressive stress, as seen from Fig. 2(c), $H_{\rm CL}$ occurs when H changes from positive to negative saturation, at the same time, $M_{\rm F}$ rotates anticlockwise from $\theta_{\rm F3}$ to $-H$, and $H_{\rm CL} < 0$ can be shown. On the other hand, it can be inferred that $H_{\rm CR}$ occurs when H varies from negative to positive saturation, meanwhile $M_{\rm F}$ rotates clockwise from $\theta_{\rm F1}$ to $+H$, and $H_{\rm CR} > 0$ will be found. Therefore, this type of loop can be classified into type Ⅲ for the reason of $H_{\rm CL} < 0$ and $H_{\rm CR} > 0$. Moreover, it can be concluded that if only the bilayer is in the bistable state for the compressive stress, i.e., in the case of Fig. 2(c), the loops with the shape of type Ⅲ will be always shown. Thus

the physical condition for the loops showing type Ⅲ is just the one for the bilayer being in the bistable state under the compressive stress.

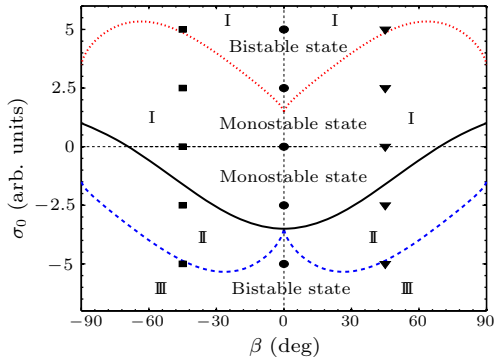

Fig. 4. (Color online) The phase diagram of the type of the hysteresis loops. The dashed and dotted lines are obtained according to Eq. (2e) and the solid line is derived by solving Eq. (3) numerically. The positions marked by the solid core squares, circles and triangles denote different parameters used in Fig. 3. The symbols I, Ⅱ and Ⅲ represent the types of the loops as illustrated in Fig. 3. The parameter $J = 2.5$ is taken in the calculations.

As far as the configurations of Figs. 2(a), 2(b) and 2(d) are concerned, $H_{\rm CR}$ occurs when H varies from zero to positive saturation, thus $H_{\rm CR} > 0$ occurs. Similarly, $H_{\rm CL}$ occurs when H varies from positive saturation to zero, and $H_{\rm CL} > 0$ will be found. Therefore, we can draw the conclusion that types I and Ⅱ of the loops will be shown in the configurations of Figs. 2(a), 2(b) and 2(d). The physical condition for discriminating type I from type Ⅱ of the loops is $H_{\rm CL} = H_{\rm CR}$, which gives us

$$\left[\frac{\sin\gamma}{A}(J\cdot\cos\beta+\cos^2\gamma)\right]^{2/3} + \left[\frac{\cos\gamma}{A}(J\cdot\cos\beta-\sin^2\gamma)\right]^{2/3} = 1. \quad (3)$$

The corresponding parameter conditions about the types of the loops are given in Fig. 4 by solving Eqs. (2d) and (3) numerically.[40]

Figure 5 gives the numerical results about the effect of the stress on $H_{\rm EB}$ and $H_{\rm C}$. Firstly, we discuss the influence of the stress orientation on the EB effect. As seen from Figs. 5(a) and 5(b), the same $H_{\rm EB}$ and $H_{\rm C}$ will be observed in some regions of β with different values of σ_0. It seems that β is not related to the EB. However, this is not the case. For a fixed σ_0, as seen from Fig. 5(a), $H_{\rm EB}$ increases with β, which means that the larger $H_{\rm EB}$ can be realized by increasing β under the same magnitude of the stress, no matter whether the compressive or tensile stress is exerted. Additionally, the overlapped region of β for the bilayers showing the same $H_{\rm EB}$ just occurs where $H_{\rm C}$ disappears. When β is fixed, if only σ_0 is in the region of type I loop, the same $H_{\rm EB}$ will always be observed, certainly, the same coercivity ($H_{\rm C} = 0$) will also be found. For example, as inferred from Fig. 4, only type-I loops will be shown for $\sigma_0 = 2.5$ and $\sigma_0 = 5$ when β varies from $-90°$ to $90°$. Hence, the results about $H_{\rm EB}$ and $H_{\rm C}$ for ($\sigma_0 = 2.5$, β) in Figs. 5(a) and 5(b) are totally the same as that for (σ_0=5, β).

As seen from Fig. 5(b), the critical orientation $\beta_{\rm C}$ is very conspicuous. It separates the zero-coercivity regions from coercive regions of β. Here $\beta_{\rm C}$ can also be derived from Eq. (3) for the given J and σ_0. The numerical result of Eq. (3) has been given by the solid lines of Fig. 4. It suggests that $\beta_{\rm C}$ decreases with the increase of the compressive stress, and the special case of $\beta_{\rm C} = 0°$ will occur at $\sigma_0 = -(1+J) = -3.5$. Hence, for $\sigma_0 < -3.5$, taking $\sigma_0 = -5$ as an example, no solution of $\beta_{\rm C}$ will be derived. It is impossible for the loops making the transition from hysteresis to anhysteresis. As seen in Fig. 4, the hysteresis loops for $\sigma_0 = -5$ will be in type Ⅱ or type Ⅲ, correspondingly, the coercivity displayed in Fig. 5(b) will not disappear anymore. As far as the tensile stress is concerned, one can see from the solid line of Fig. 4 that $\beta_{\rm C}$ will disappear for $\sigma_0 > 1$, which can be derived from Eq. (3) under the condition of $\beta_{\rm C} = 90°$. This also means that the transition of the loops from $H_{\rm C} = 0$ to $H_{\rm C} \neq 0$ will not take place. As seen in Fig. 4, only type-I loops will be shown for $\sigma_0 > 1$. Therefore, for $\sigma_0 = 2.5$ and $\sigma_0 = 5$, as seen in Figs. 5(a) and 5(b), only $H_{\rm EB}$ is shown, while $H_{\rm C}$ is always kept at the value of zero.

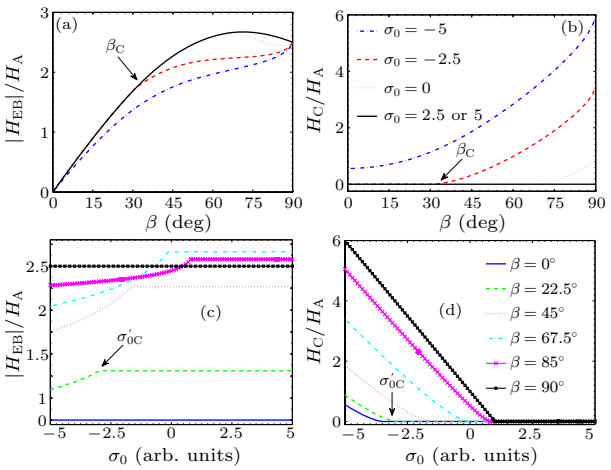

Fig. 5. The effect of the various mechanical stresses on the exchange bias field $H_{\rm EB}$ and the coercivity $H_{\rm C}$. The parameter $J = 2.5$ is taken in the calculations. The critical values of σ_0 and β are indicated by arrows.

Now we turn to Figs. 5(c)and 5(d). When β is fixed and σ_0 is varied from -5 to $+5$, $H_{\rm EB}$ will increase with the decreasing compressive stress and it continues to increase until reaching a peak value at the critical stress $\sigma'_{0\rm C}$. During this varied process of the stress, $H_{\rm C}$ will make a continuous decrease until it vanishes at $\sigma'_{0\rm C}$. Then, both $H_{\rm EB}$ and $H_{\rm C}$ will keep constant for $\sigma_0 > \sigma'_{0\rm C}$. Likewise, the determined equation of $\sigma'_{0\rm C}$ is also given by Eq. (3), and the relationship between $\sigma'_{0\rm C}$ and β has also been given by the solid line of Fig. 4.

However, there is also an exceptional case: $H_{\rm EB}(\sigma_0)$ curves for $\beta = 0°$ and $\beta = 90°$ present a hor-

izontal line, which is different from the other results. This indicates that H_{EB} is kept constant, which is consistent with the previous works.[33,34] As reported by Han *et al.*,[34] H_{EB} will not be apparently changed when σ is applied parallel or perpendicular to the easy axis (EA) of K_U and K_E. As seen from Fig 2(b) of their work ($\sigma//$EA and $H\perp$EA, which is equivalent to $\beta = 0°$), $H_{EB} = 0$ can be found no matter whether the compressive or tensile stress is applied. On the other hand, H_C is increased when the bilayer is in the tensile-stress state and it nearly vanishes for the nonstressed and compressive-stress states.[34] However, for $\beta = 0°$ of Fig. 5(d), H_C is increased with the compressive stress and it keeps at zero for $\sigma_0 \geq 0$. If one considers the negative magnetostriction in their work,[34] our result for $\beta = 0°$ is consistent with their experimental observations, due to the fact that the effect of the compressive (tensile) stress for the positive magnetostriction is equivalent to that of the tensile (compressive) stress for the negative magnetostriction.[24–26]

Similarly, one can see from Fig. 3(a) of the work of Han *et al.*[34] ($\sigma\perp$EA and $H//$EA, which correspond to $\beta = 90°$), $H_{EB} \neq 0$ is found and it nearly keeps a constant value, which is consistent with $\beta = 90°$ of Fig. 5(c). Additionally, H_C shown in Fig. 3(a) of their work[34] is increased for the tensile stress and it is decreased for the compressive stress, respectively. On the contrary, H_C is increased for the compressive stress as shown in Fig. 5(d) for $\beta = 90°$, and it is decreased for the tensile stress (even, H_C will vanish itself when σ_0 is above σ'_{0C}), respectively. Again, considering the converse magnetostriction, our result is also consistent with their experimental observations.

Furthermore, we can also make a comparison between our numerical results and the results of Zhang *et al.*[33] Substituting $J = 2.5$ and $\beta = 85°$ into Eq. (3), the critical stress can be obtained as $\sigma'_{0C} = 0.8071$, which indicates that $H_\sigma = K_\sigma/M_F = (2K_U/M_F) \cdot (K_\sigma/2K_U) = 0.5 \cdot H_A \cdot \sigma_0 = 0.5 \times 40 \times 0.8071 = 16.142$ Oe. This calculated result approaches to their report that $H_\sigma \sim 16$ Oe.[33]

In summary, we have performed a theoretical investigation about the influence of the mechanical stress on the exchange bias effect when the FM/AFM bilayer is deposited on the flexible substrate. Three different types of the hysteresis loops can be found, and the physical conditions for each type of the loop are deduced based on the principle of minimal energy. Both the magnitude and orientation of the stress affect the exchange bias effect significantly. Our analyses made in this work will be useful to control or tune the exchange bias effect by introducing various stress into the FM/AFM bilayer.

References

[1] Meiklejohn W H and Bean C P 1956 *Phys. Rev.* **102** 1413
[2] Dieny B et al 1991 *Phys. Rev.* B **43** 1297
[3] Heim D et al 1994 *IEEE Trans. Magn.* **30** 316
[4] Nogués J and Schuller I K 1999 *J. Magn. Magn. Mater.* **192** 203
[5] Stamps R 2000 *J. Phys.* D **33** R247
[6] Kiwi M 2001 *J. Magn. Magn. Mater.* **234** 584
[7] Nogues J et al 2005 *Phys. Rep.* **422** 65
[8] Giri S et al 2011 *J. Phys.: Condens. Matter* **23** 073201
[9] O'Grady K et al 2010 *J. Magn. Magn. Mater.* **322** 883
[10] Shi Z et al 2014 *Chin. Phys.* B **23** 027503
[11] Chung S H et al 2005 *Phys. Rev.* B **71** 214430
[12] Tillmanns A E and Blachowicz T 2011 *J. Appl. Phys.* **109** 083923
[13] Jiménez E et al 2009 *Appl. Phys. Lett.* **95** 122508
[14] Mewes T et al 2002 *Phys. Rev.* B **65** 224423
[15] Geshev J et al 2008 *Phys. Rev.* B **77** 132407
[16] McCord J, Hamann C, Schäfer R, Schultz L and Mattheis R 2008 *Phys. Rev.* B **78** 094419
[17] Dijken S V, Santo G D and Poelsema B 2001 *Phys. Rev.* B **63** 104431
[18] Rodríguez-Suárez R L, Vilela-Leão L H, Landeros P and Azevedo A 2012 *Appl. Phys. Lett.* **100** 242406
[19] Zhang Y, Zhan Q F, Zuo Z G, Liu Y W, Yu Y, Wang J, Wang B M and Li R W 2015 *Phys. Rev.* B **91** 174411
[20] Yang C C, Zhang C, Wang F L, Zhao Z, Jiang C J and Xue D S 2015 *Appl. Phys.* A **120** 1159
[21] Brooks M, Summers E, Restorff J B and Wun-Fogle M 2012 *J. Appl. Phys.* **111** 07A907
[22] Mathews M, Jansen R, Rijnders G, Lodder J C and Blank D H A 2009 *Phys. Rev.* B **80** 064408
[23] Liedke M O, Liedke B, Keller A, Hillebrands B and Mücklich A 2007 *Phys. Rev.* B **75** 220407(R)
[24] Dai G H, Zhan Q F, Liu Y W, Chen B and Li R W 2012 *Appl. Phys. Lett.* **100** 122407
Dai G H, Zhan Q F, Liu Y W, Chen B and Li R W 2013 *J. Appl. Phys.* **114** 173913
[25] Yu Y, Zhan Q F, Wei J W, Wang J B, Dai G H, Xie S H, Wang B M and Li R W 2015 *Appl. Phys. Lett.* **106** 162405
[26] Tang Z H, Wang B M, Yang H L, Liu Y W, Zhan Q F, Zhou Y C, Wang J L and Li R W 2014 *Appl. Phys. Lett.* **105** 103504
[27] Zhang H, Li Y Y, Yang M Y, Zhang B, Yang G, Wang S G and Wang K Y 2015 *Chin. Phys.* B **24** 077501
[28] Chen A, Zhao Y, Li P, Peng R, Miao P, Cai J W and Nan C W 2016 *Adv. Mater.* **28** 363
[29] Yang C C, Wang F L, Zhang C, Zhou C and Jiang C J 2015 *J. Phys. D: Appl. Phys.* **48** 435001
[30] Li P S, Chen A T, Li D L, Zhao Y G, Zhang S, Yang L F, Liu Y, Zhu M H, Zhang H Y and Han X F 2014 *Adv. Mater.* **26** 4320
[31] Liu M, Lou J, Li S D and Sun N X 2011 *Adv. Funct. Mater.* **21** 2593
[32] Dong C H, Guo D W, Jiang C J, Jia C L and Xue D S 2014 *Appl. Phys. Lett.* **104** 062403
[33] Zhang X S, Zhan Q F, Dai G H, Liu Y W, Zuo Z G, Yang H L, Chen B and Li R W 2013 *Appl. Phys. Lett.* **102** 022412
[34] Han D H, Zhu J G, Judy J H and Sivertsen J M 1997 *Appl. Phys. Lett.* **70** 664
[35] Han D H, Zhu J G, Judy J H and Sivertsen J M 1997 *J. Appl. Phys.* **81** 4519
[36] Bai Y H, Yun G H and Bai N 2009 *Acta Phys. Sin.* **58** 4962 (in Chinese)
[37] Guo Z Z 2011 *Solid State Commun.* **151** 116
Guo Z Z 2013 *Acta Phys. Sin.* **62** 057501 (in Chinese)
[38] Camarero J, Sort J, Hoffmann A, Garcia-Martin J M and Dieny B 2005 *Phys. Rev. Lett.* **95** 057204
[39] Bai Y H, Yun G H and Bai N 2009 *J. Appl. Phys.* **106** 063919
Bai Y H, Yun G H and Bai N 2010 *J. Appl. Phys.* **107** 033905
[40] Yang H P and Bai Y H 2014 *Physica* B **433** 12
Yang H P and Bai Y H 2014 *Chin. Phys. B* **23** 067503
[41] Radu F, Westphalen A, Theis-Bröhl K and Zable H 2006 *J. Phys.: Condens. Matter* **18** L29
[42] Oliveira B, Rodriguez-Suarez R, Michea S and Denardin J 2014 *J. Appl. Phys.* **116** 033910